Journal of Colloid and Interface Science 637 (2023) 489–499

Contents lists available at ScienceDirect

Journal of Colloid and Interface Science

journal homepage: www.elsevier.com/locate/jcis

Surface hydrophilicity-mediated migration of nano/microparticles under temperature gradient in a confined space

Haolan Xu [a,c], Xu Zheng [b,*], Xinghua Shi [a,c,*]

[a] Laboratory of Theoretical and Computational Nanoscience, CAS Center for Excellence in Nanoscience, National Center for Nanoscience and Technology, Chinese Academy of Sciences, Beijing 100190, China
[b] State Key Laboratory of Nonlinear Mechanics, Institute of Mechanics, Chinese Academy of Sciences, Beijing 100190, China
[c] University of Chinese Academy of Sciences, No.19A Yuquan Road, Beijing 100049, China

GRAPHICAL ABSTRACT

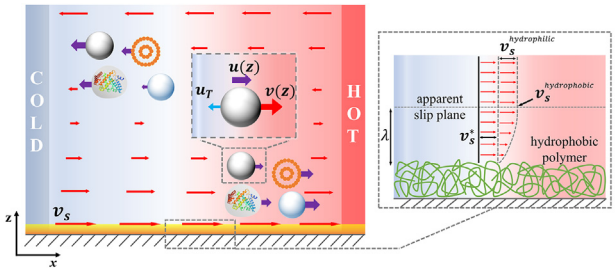

ARTICLE INFO

Article history:
Received 25 November 2022
Revised 17 January 2023
Accepted 22 January 2023
Available online 26 January 2023

Keywords:
Thermophoresis
Thermo-osmosis
Soret coefficient
Hydrophobicity
Nanoparticle

ABSTRACT

Hypothesis: Particle transport by a temperature gradient is prospective in many biomedical applications. However, the prevalence of boundary confinement in practical use introduces synergistic effects of thermophoresis and thermo-osmosis, causing controversial phenomena and great difficulty in understanding the mechanisms.

Experiments: We developed a microfluidic chip with a uniform temperature gradient and switchable substrate hydrophilicity to measure the migrations of various particles (d = 200 nm – 2 μm), through which the effects of particle thermophoresis and thermo-osmotic flow from the substrate surface were decoupled. The contribution of substrate hydrophilicity on thermo-osmosis was examined. Thermophoresis was measured to clarify its dependence on particle size and hydrophilicity.

Findings: This paper reports the first experimental evidence of a large enthalpy-dependent thermo-osmotic mobility $\chi \sim \Delta H$ on a hydrophobic polymer surface, which is 1–2 orders of magnitude larger than that on hydrophilic surfaces. The normalized Soret coefficient for polystyrene particles, S_T/d = 18.0 $K^{-1}\mu m^{-1}$, is confirmed to be constant, which helps clarify the controversy of the size dependence. Besides, the Soret coefficient of hydrophobic proteins is approximately-four times larger than that of hydrophilic extracellular vesicles. These findings suggest that the intrinsic slip on the hydrophobic surface could enhance both surface thermo-osmosis and particle thermophoresis.

* Corresponding authors at: Laboratory of Theoretical and Computational Nanoscience, CAS Center for Excellence in Nanoscience, National Center for Nanoscience and Technology, Chinese Academy of Sciences, Beijing 100190, China (X. Shi).
E-mail addresses: zhengxu@lnm.imech.ac.cn (X. Zheng), shixh@nanoctr.cn (X. Shi).

https://doi.org/10.1016/j.jcis.2023.01.112
0021-9797/

1. Introduction

The temperature gradient can work as a generalized force driving molecules or particles in the solution to move along the gradient. This thermal transport phenomenon, known as thermophoresis, has been investigated and considered to be an important mechanism in many applications, such as DNA trapping [1,2], micro/nanomotors [3,4], binding affinity/kinetics measurement [5,6], thermophoresis therapy [7,8], and particle manipulation [9–14]. In particular, the thermophoretic sensor based on the lab-on-a-chip technique provides a noninvasive and effective method for the rapid identification of viral pathogens [15] and early cancer diagnosis [16,17], and emerging techniques like opto-thermophoretic manipulation and photothermal nanorobots can achieve particle transport and multi-functions by the temperature gradient originating from the optical heating [9–13,18–20]. The applications based on the thermal manipulation of particles have attracted considerable attention.

The origin of the thermophoresis is closely related to interfacial hydrodynamics [21–25]. Unlike the macroscopic flow driven by body force or pressure gradient, the particle thermophoresis on the micro- and nanoscales is caused by the temperature gradient near the particle–fluid interface. In the past two decades, many experiments on thermophoresis in various solutions manifested rich physics and reported controversial and surprising phenomena due to the complexity [25–38]. In electrolyte solutions the excess hydrostatic pressure and electrostatic thermopotential in the electric double layer dominate the ion transport and the corresponding interfacial flow [39,40], while in complex fluids containing polymer or other macromolecules, the entropic effect, such as depletion effects could be more significant [35]. On the other hand, owing to the difficulty of quantifying the microscopic mechanisms and the coupling of the above multi-field effects, it is a great challenge to clarify the existing controversy of thermophoresis experiments. The controversial results of some fundamental issues have puzzled researcher for many years, such as the debate of thermophilic or thermophobic behavior of specific nanoparticles [33,38,41], the scattered results of the Soret coefficient that characterizing the thermophoretic mobility and its dependence of physical factors.

On top of the mechanism debates, the growing demand and progress of new techniques based on thermophoresis of various nano/microparticles have attracted widespread attention because of the advantage that the temperature gradient effect becomes efficient on the microscale [6–12,15–17]. One ongoing development of thermophoresis-based biomedical detection is integrating the thermophoretic manipulation and sensing functions into a microfluidic chip [11,15,17]. Microfluidic manipulation usually works in a confined space. Similar to the mechanisms occurring on the particle interface mentioned above, interfacial flow occurs on the confinement wall along the temperature gradient, which is called thermo-osmosis [22]. Inevitably, we would ask: How does this interfacial flow on the wall influence the particle migration near the wall, or how can the contribution of thermo-osmosis and particle thermophoresis be distinguished? This issue is fundamentally important because in applications like lab-on-a-chip techniques, particle transport or manipulation prevalently occurs in a confined space. In particular, in the emerging technique of opto-thermophoretic manipulation and temperature-mapping nano-thermometry where interfacial flow plays a key role [13,42], the performance could be affected severely by the synergistic effects of particle thermophoresis and hydrodynamic flow arising from the thermo-osmosis of a nearby surface. In contrast, the contribution of both effects and the mechanism of tuning the interfacial thermo-osmosis remain unclear.

Thermo-osmosis has been described through hydrodynamics descriptions with a proper apparent slip boundary condition [22]. Until recently, Bregulla *et al.* reported the first microscale observation of fluid flows caused by thermo-osmosis along the solid-liquid boundary [43]. They showed that the thermodynamic properties of the surface are crucial for determining the thermo-osmotic mobility. New progress further suggested that the intrinsic fluid slip on the interface could play a role in influencing the particle migration nearby [43,44]. These results called for more careful experiments to characterize the thermo-osmotic effect at various interfaces and reconsider the coupling of thermo-osmosis and particle thermophoresis. Yet so far, effects of surface hydrophilicity and its contribution to the thermophoretic motion of various particles remain mysterious.

Therefore, we design a microfluidic chip with a controlled temperature gradient and switchable substrate hydrophilicity to investigate the thermal migration of various nano/micro particles. We decipher the effects of interfacial thermo-osmosis and particle thermophoresis, and unveil the surprisingly large thermo-osmotic velocity on the hydrophobic polymer surface that is almost two orders of magnitude larger than the reported thermo-osmotic velocity on the hydrophilic glass surface. Our result shows a constant normalized Soret coefficient, which could help resolve the controversy of the thermophoresis mechanisms in a confined space and determine the size dependence of the Soret coefficient. The average temperature in the middle part of our microfluidic chip is always 36.1 °C, which is very close to human body temperature, suggesting the potential implementation of the chip for manipulating bio-particles. As a demonstration, we measure the thermophoresis of protein granules and extracellular vesicles (EVs), and find a large difference in their thermophoretic mobilities, implying the possibility of using thermophoresis to separate various bio-particles.

2. Materials and methods

2.1. Microfluidic chip fabrication

The microfluidic chip was made of stainless steel and contained three channels (Fig. 1a), similar to a previous study [45–47] with some modifications. Theoretical analysis (Supplementary material S1) was conducted to explain the working mechanism and optimize the design of a microfluidic chip as well. A constant temperature gradient was established in the central microchannel $\boldsymbol{a}$ (width = 200 μm, depth = 50 μm, and length = 28 mm) by the circulation of hot (80 ℃) and cold (0 ℃, ice-water mixture) water in the two side channels $\boldsymbol{b}_1$ and $\boldsymbol{b}_2$ (width = 2 mm, depth = 2 mm, length = 28 mm), respectively. The flows in two side channels were in opposite directions so that the temperature gradient along the transverse direction (defined as the x-axis) of the microchannel was more uniform. The temperature gradient is controlled by adjusting the flow rates of cold and hot water in both side channels. To reduce heat leakage, a deep slit $\boldsymbol{c}$ is cut below the central channel. $\boldsymbol{d}_1 - \boldsymbol{d}_4$ are the entrances used to connect pipes for cold and hot water. $\boldsymbol{d}_5$ and $\boldsymbol{d}_6$ are entrances of the central microchannel. The microfluidic chip was sealed with an optical adhesive film (MicroAmp™), which is convenient for fabrication and surface modification. The original film was hydrophobic as the measured contact angle was approximately 110° (Supplementary material S2, Fig. S5a). After treatment with plasma cleaner (Harrick Plasma, PDC-32G) for ∼150 s, the film surface was modified to be hydrophilic, and the contact angle was approximately 40° (Supplementary material S2, Fig. S5b).

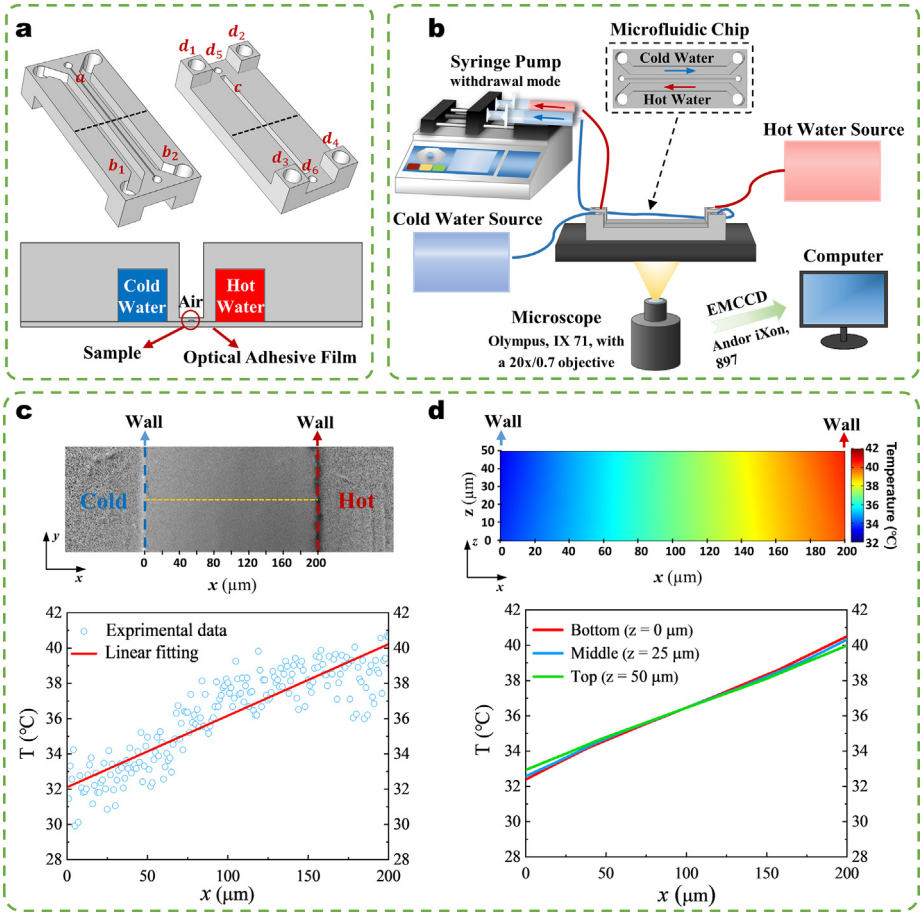

Fig. 1. (a) Schematic diagram of the microfluidic chip. The top panels show the bottom (left) and top (right) views of the microfluidic chip. (b) Schematic diagram of the experimental setup. (c-d) Temperature profiles along the transverse direction in the central microchannel when Q = 5 mL/min. (c) Experimental results. Top panel: the normalized fluorescence intensity of the temperature sensitive fluorescence Rhodamine B, bottom panel: the corresponding temperature profile. Axes x and y denote the transverse and streamwise directions of the central microchannel. (d) Simulation results. Top panel: the temperature field in the microchannel cross-section (z-axis is the height direction). Bottom panel: the temperature distributions at various heights of the microchannel.

2.2. Experimental setup

The experimental setup is illustrated in the Fig. 1b. A dual-channel syringe pump (Longer Pump LSP02-1B) was used to control the flow rate (5 – 15 mL/min) of hot (80 ℃) and cold (0 ℃, ice-water mixture) water simultaneously. The syringe pump worked in a withdrawal mode and pumped water from both water sources whose temperatures were monitored by thermometers. The maximum temperature gradient was up to $\nabla T = 6.04 \times 10^4$ K/m (corresponding to a 12.1 K temperature difference across the microchannel) by the flow rates of Q = 15 mL/min for both hot and cold water. An inverted fluorescence microscope (Olympus, IX 71) with a 20×/0.7 objective was used for the experimental observations. An EMCCD (Andor iXon, Ultra897) was used to capture experimental images at a frame rate of 2 fps. All the experiments were performed at room temperature 22.0 ℃ ± 1.0 ℃. The substrate wall position z = 0 μm was determined by the particles that adhere to the bottom substrate [48,49]. By using a piezo transducer mounted under the microscopic objective, we could accurately adjust the focus plane and determine its z position with a displacement precision of 0.1 μm.

2.3. Particle sample preparation

Various particles with a wide range of diameters and different surface properties were prepared. Fluorescent polystyrene (PS) particles (d = 0.2, 0.5, 0.71, 1.0 and 2.0 μm, Thermo-Fisher Scientific) and silica particles (d = 0.5 μm, sicastar®-greenF) were used in the experiments, which have pendent carboxylic acids on their surface. Before experiments, all particle suspensions were diluted to 0.01 – 0.1 wt% with DI water (Milli-Q, 18.2 MΩ·cm). All particles used in this work are fluorescent, including commercial fluorescent polystyrene particles, and other particles (silica, proteins and extracellular vesicles) labeled with fluorescence in our lab.

The PGL-3 granules were assembled by liquid–liquid phase separation (LLPS). The PGL-3::mCherry proteins were dissolved in a buffer solution (pH 7.5) containing 20 mM HEPES and 500 mM NaCl. In a T-type microfluidic chip, phase separation occurred when this mixture was diluted with a low-salt buffer (20 mM HEPES and 100 mM NaCl, pH 7.5), and the PGL-3::mCherry proteins formed condensed granules. The granules with a diameter of approximately 1.5 – 2.0 μm were collected for the thermal migration experiment.

The mesenchymal stem cell EVs were prepared by different ultracentrifugation at 4℃. The cell culture supernatant containing EVs was first centrifuged at 800g for 5 min, then by additional centrifugation at 2000g for 20 min. Further purification was performed by membrane filtration (0.8 μm; Millipore) in a type Ti70 rotor using an XPN-1000 ultracentrifuge (Beckman Coulter, Brea, CA, USA), centrifuged at 150,000 g for 90 min. For better visualization, the EVs were labeled with green fluorescent lipid dye PKH-67.

2.4. Particle tracking

The particle tracking method measured the migration of particles driven by the temperature gradient based on the observation by an inverted fluorescence microscope (Olympus IX71). An EMCCD (Andor iXon, Ultra897) was used to record the images. Image analysis was performed using ImageJ software and its plugin Particle Tracker, through which the positions and displacements of particles in the image series were obtained. The particles mainly moved in the horizontal direction following the temperature direction, however, they could also move in vertical z direction due to Brownian motion. To make sure the measured velocity represented the typical motion in a fixed z position, we excluded the particles that moved far from the focus plane at the same z position by choosing a proper threshold greyscale value. Therefore, only the particles that stayed close to the focus plane for sufficiently long time were tracked and taken into calculation. To reduce the influence of Brownian motion as much as possible, the sampled amount of particle number in each experiment exceeded 100, and for each particle the observation time reached 100 – 200 s, corresponding to 200 – 400 frames. In addition, the circulating flow in the cross-section of the microchannel can also introduce particles' motion in z direction. To avoid this influence, we only tracked the particles in the middle region (50 μm $\leq x \leq$ 150 μm, as shown by the red rectangular in Fig. 3e) of the microchannel.

2.5. Temperature field characterization

The temperature profile in the central microchannel was measured using a temperature-sensitive fluorescence Rhodamine B (0.1 mM, #83689, Sigma–Aldrich) [50]. When the flow rates of hot and cold water in the two side channels were set to Q = 5 mL/min, the normalized fluorescence intensity $I(T)$ was recorded by the EMCCD (top panel of Fig. 1c). The measured temperature profile along the × direction is shown in the bottom panel of Fig. 1c, based on a predetermined polynomial equation (Supplementary material S3). The measured temperature difference was approximately 8.1 K, corresponding to a temperature gradient $\nabla T = 4.05 \times 10^4$ K/m, which is in excellent agreement with the simulation result (Fig. 1d, Supplementary material S1). The top panel of Fig. 1d is the temperature field in the microchannel cross-section obtained by simulation, and the bottom panel shows the temperature variations along the x-axis at various heights of the microchannel. The temperature profiles in different heights of the microchannel are very uniform and approximately the same. Thus, the thermophoresis of the particle is expected to be the same and independent of the z position. Compared with previous thermophoretic measurements using heating focus from laser [28,29,35], the setup builds a stable temperature field for clarifying the thermophoretic mechanism.

3. Results and discussion

3.1. Peculiar coexistence of thermophilic and thermophobic migration of particles

We systematically investigated the migration of various nano and microparticles with different sizes and compositions in the microfluidic chip under a controlled temperature gradient. First, we observed intriguing thermophilic behavior independent of particle composition, which could assist in particle separation under the same temperature gradient. When the observation occurred near the hydrophobic substrate at z = 1 μm, we found that the PS particles (Fig. 2a and 2b, d = 2 μm) moved from the cold side to the hot side. After applying the temperature gradient of $\nabla T = 4.0 \times 10^4$ K/m for 5 mins, the PS particles accumulated on the hot side near the microchannel sidewall, suggesting a potential microfluidic enrichment method for particles. We used PS particles with diameter ranging from 0.2 to 2.0 μm and obtained the same migration direction. The enrichment could be accelerated by applying higher temperature gradient if the flow rates of the cold and hot water were increased in both side channels. The experiments were then performed using silica particles, in which similar thermophilic migration was noted with a slightly larger speed to the hot side.

However, the above thermophilic behavior of PS particles was opposite to many existing results [29,30,41], which reported thermophobic migration of PS particles. The inconsistency was examined by measuring the particle migration velocity by levitating the observation plane, *i.e.*, the focus plane of the objective of the microscope, to different z positions. Surprisingly, we find reversed direction of particle migration in the middle and upper region of the microchannel. Fig. 2c and 2d show the moving trajectories of 710 nm PS particles at vertical positions z = 1 μm and 25 μm, respectively. The PS particles became thermophobic in the middle of the microchannel at z = 25 μm, manifesting an average speed toward the cold side of approximately 0.7 μm/s, in contrast to their average thermophilic speed of approximately 0.7 μm/s to the hot side at the plane of z = 1 μm. Similar phenomena were observed while using 1 μm PS particles, as shown in Fig. 2e and 2f. Compared with the enrichment of 2 μm particles shown in Fig. 2b, the enrichment is less effective when the particle sedimentation effect becomes weak for smaller sizes. From Movie S1 & S2, one can easily observe the existence of a circulation transport that lifts the smaller PS particles upwards from their accumulation near the hot side (z = 1 μm) and transport the particles downwards near the cold side (z = 25 μm). Such counter-clockwise circulation transports in the microchannel cross-section were prevalent in our experiments regardless of whether PS or silica particles were used. The thermal convection caused by density difference can be neglected in this work, because of the shallow geometry (h = 50 μm) of the microchannel. In the COMSOL simulation, we found that the typical convective velocity is about 10^{-2} μm/s, which is much smaller than the thermophoretic velocity of particles and the thermo-osmotic velocity in our experiments. These findings suggest that thermophoresis should not be the only mechanism controlling the particle migration. Given that under the temperature gradient there should be an interfacial thermo-osmotic flow generated simultaneously on the substrate, this paper proposes that the hydrodynamic creep flow originating from this interfacial thermo-osmosis causes the circulation transport of particles.

The argument of the interfacial thermo-osmosis was verified by varying the hydrophilicity of the substrate. After plasma treatment of the film surface, the substrate became hydrophilic, and the experiment was commenced immediately. The experimental result showed a much slower thermophilic migration near the hydrophilic surface, as shown by the trajectories in Fig. 3a and 3b. The measured migration speed of 710 nm and 1 μm PS particles near hydrophilic substrate are also provided in Fig. 3c (open symbols with dash curves). The comparison in Fig. 3c clearly shows that the average migration speed (∼0.25 μm/s) near the hydrophilic substrate was reduced to approximately 30 % of the average speed (∼0.7 μm/s) near the hydrophobic substrate. This result evidences the hydrophilicity-suppressed thermophilic migration of particles near the substrate, which should be attributed to the lower interfacial thermo-osmosis on the hydrophilic surface.

This phenomenon is reminiscent of a recent study showing that interfacial thermo-osmosis can be significantly weakened by changing surface properties [43]. Our observation is qualitatively in agreement with their results, verifying the important contribution of the thermo-osmotic flow originating from the substrate,

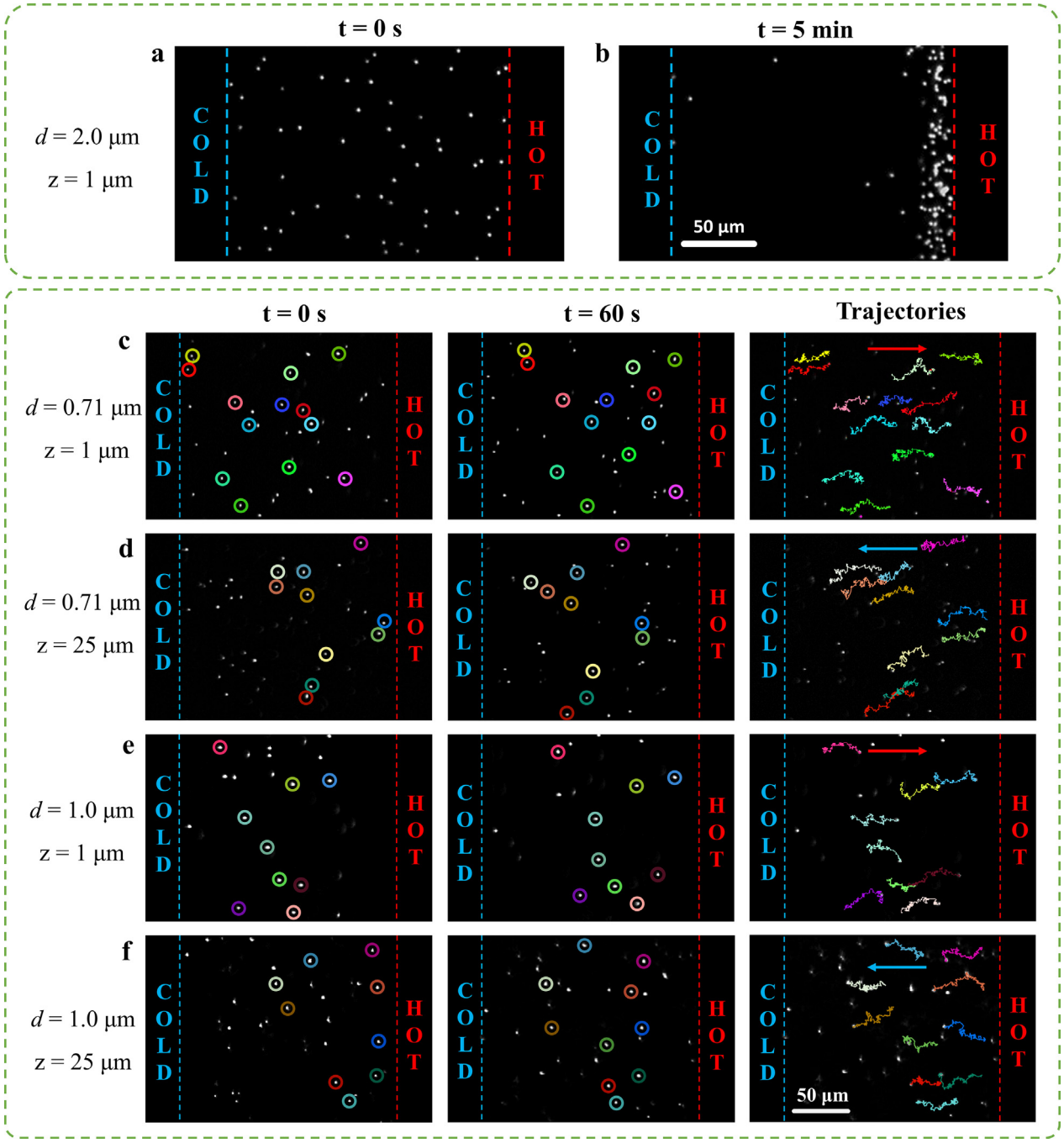

Fig. 2. (a-b) Enrichment of 2 μm PS particles by their thermophilic migrations near the hydrophobic substrate. (a) Before applying the temperature gradient, the PS particles were distributed in the microchannel uniformly and randomly. (b) After applying a temperature gradient $\nabla T = 4.05 \times 10^4$ K/m for 5 min, the PS particles were accumulated on the hot side. (c-f) Peculiar coexistence of thermophilic and thermophobic migration under the same temperature gradient in the same microchannel. (c-d) The experimental results of 710 nm PS particles at (c) $z = 1$ μm near the hydrophobic substrate, and at (d) $z = 25$ μm in the middle of the channel (Movie S1 & 2). (e-f) The experimental results of 1 μm PS particles at (e) $z = 1$ μm near the hydrophobic substrate, and at (f) $z = 25$ μm in the middle of the channel. The first column is the snapshots before applying the temperature gradient at $t = 0$ s. The second column is the snapshots after applying the temperature gradient for $t = 60$ s. Colorful circles are used to mark those tracked particles. The tracking trajectories for 60 s are shown in the third column. In both cases, the particle migrations near the hydrophobic substrate are thermophilic, toward the hot side on the right [(c, e)]; the particle migrations in the middle of the channel are thermophobic, toward the cold side on the left [(d, f)], and the arrows indicate the migration direction of particles. The fluctuation of the trajectory is due to Brownian motion of the particle.

particularly a hydrophobic substrate. Moreover, changing the substrate surface to hydrophilic reduces the particle speed near the substrate and weakens their transport in the middle of the microchannel. The experimental results indicate that the underlying mechanisms of particle migration $u(z)$ in the microchannel are twofold. In addition to the thermophoresis $\boldsymbol{u}_T$ of the particles, the hydrodynamic flow $v(z)$ because of the interfacial thermo-osmosis v_s should also be considered (Fig. 3d).

3.2. Decouple the effects of particle thermophoresis and interfacial thermo-osmosis

The effects of particle thermophoresis and interfacial thermo-osmosis were decoupled to explain the above experimental findings. We use Fig. 3d to schematically explain that the particle migration velocity $u(z)$ is composed of the contribution from the hydrodynamic creep flow $v(z)$ caused by the interfacial thermo-

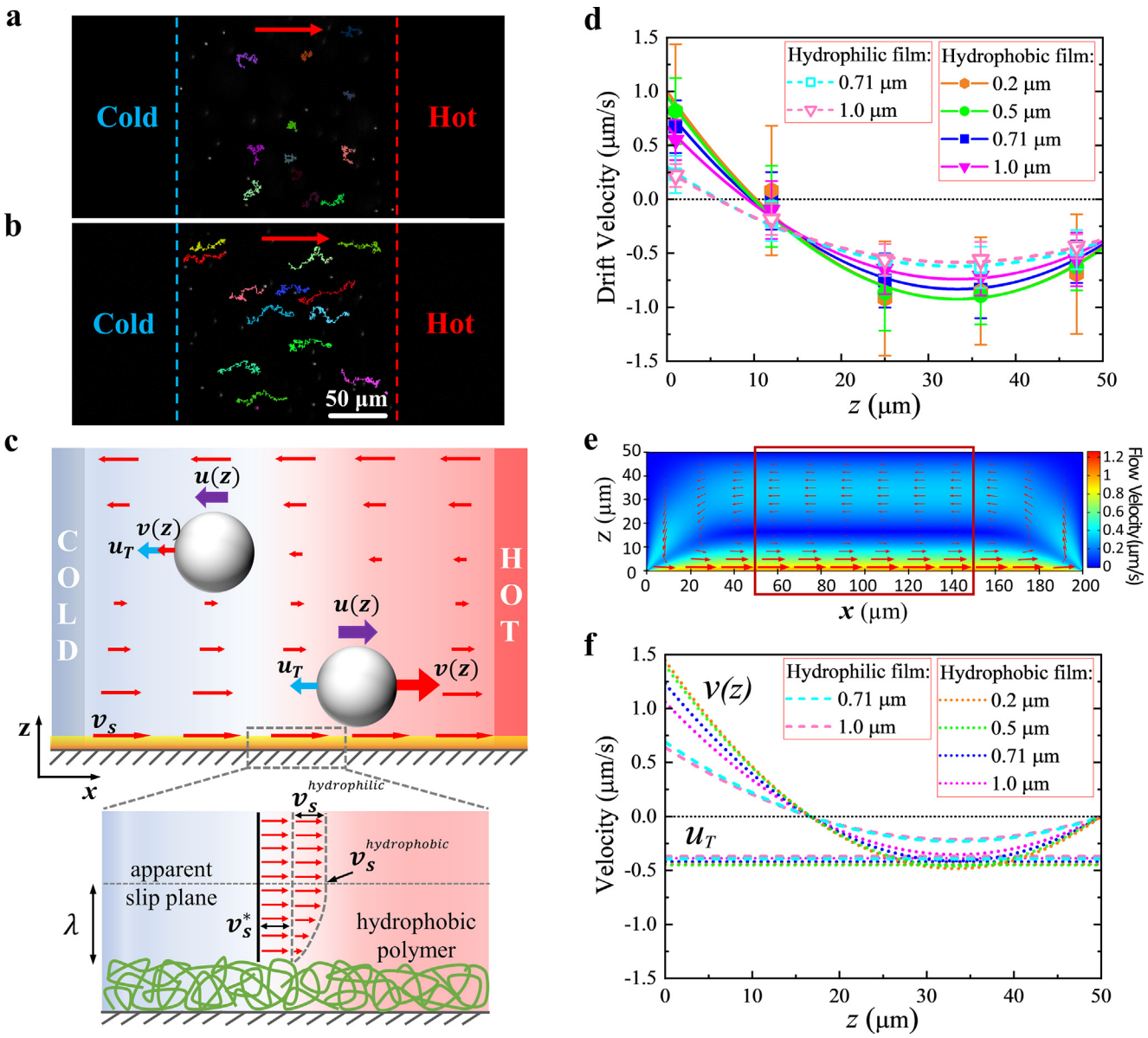

Fig. 3. (a-b) Comparison of 710 nm PS particle migration near (a) a hydrophilic substrate surface and (b) a hydrophobic one (Movie S1 & 3). The duration is 60 s. The arrows indicate the migration direction of particles. (c) The measured migration velocity $u(z)$ of different PS particles at different heights of the microchannel. The symbols are experimental data, and the lines are the fitting curve of Eq. (6). The temperature gradient is $\nabla T = 4.05 \times 10^4$ K/m. The error bars represent the standard deviations of the measured data. (d) Top panel: a schematic diagram is provided to show that the particle migration velocity $u(z)$ is composed of the contribution from the hydrodynamic creep flow $v(z)$ caused by the interfacial thermo-osmosis and the particle thermophoresis $\boldsymbol{u}_T$. The coexistence of thermophilic and thermophobic behaviors can be understood based on competition between the effects of interfacial thermo-osmosis and the particle thermophoresis. Bottom panel: the apparent thermo-osmotic velocity $v_s^{hydrophobic}$ close to a hydrophobic polymer surface. Compared to the thermo-osmotic velocity $v_s^{hydrophilic}$ near a hydrophilic polymer surface, $v_s^{hydrophobic}$ is enhanced by the contribution of v^*_s caused by intrinsic fluid slip on a hydrophobic polymer surface. (e) Hydrodynamic creep flow field in the cross-section of the central microchannel caused by a thermo-osmotic velocity $v_s = 1.24$ μm/s on the bottom interface is obtained by simulation. Note that $v_s = 1.24$ μm/s is the fitted value based on the experimental data using 710 nm particles near the hydrophobic surface. The red rectangular indicates the region where particle velocity was measured (50 μm $\leq x \leq$ 150 μm). (f) The decoupled results show consistent particle thermophoresis $\boldsymbol{u}_T$, and different parabolic velocity profiles $v(z)$ dominated by surface hydrophilicity. (For interpretation of the references to colour in this figure legend, the reader is referred to the web version of this article.)

osmosis and the particle thermophoresis $\boldsymbol{u}_T$, which is expressed as follow:

$$u(z) = \boldsymbol{u}_T + v(z) \tag{1}$$

The thermophoretic velocity is only related to the thermophoretic mobility D_T under a constant temperature gradient ∇T:

$$\boldsymbol{u}_T = -D_T \nabla T \tag{2}$$

For PS particles, they should move from the hot side to the cold side at the experimental temperature [29,30,41], defined as positive thermophoresis (thermophobic) with $D_T > 0$ and $\boldsymbol{u}_T < 0$. A uniform temperature gradient ∇T along the microchannel height means $\boldsymbol{u}_T$ is constant and independent of z. Therefore, characterizing the coexistence of the apparently thermophilic and thermophobic migrations relies on determining the hydrodynamic flow field $v(z)$ caused by interfacial thermo-osmosis.

To clarify the contribution of the thermo-osmosis, we briefly review its origin and advance. The thermo-osmotic flow driven by a temperature gradient along an interface was first analyzed by Derjaguin *et al.* [22]. They related the thermo-osmosis to the excess enthalpy h, resulting in the apparent slip velocity v_s on the interface:

$$v_s = -\frac{1}{\eta}\int_0^\infty dz h(z)\frac{\nabla T}{T} = \chi\frac{\nabla T}{T} \tag{3}$$

where η is viscosity and χ is the thermo-osmosis coefficient. According to Eq. (3), the direction of the apparent slip flow depends on the enthalpy $h(z)$ of the interfacial layer. The thermo-osmotic flow moves to a lower temperature when $h(z) > 0$, and moves to a higher temperature when $h(z) < 0$. The value and sign of enthalpy h depend on the physicochemical properties of the surface.

Generally, the electrostatic force in the electric double layer results in a negative enthalpy and drives the fluids to the hot side ($\chi > 0$) [21,43]. Within the Debye–Hückel approximation, we have [43]:

$$v_s = \chi\frac{\nabla T}{T} = \frac{\varepsilon\zeta^2}{8\eta}\frac{\nabla T}{T} \tag{4}$$

where ε is permittivity and ζ is surface potential. Eq. (4) was applied to the upper metallic surface where electrostatic force in the double layer is dominant, and obtain $v_s \sim 10^{-2}$ μm/s and $\chi \sim 10^{-10}$ m^2/s by substituting $\zeta \sim$ -30 mV and $\nabla T = 4.05 \times 10^4$ K/m. This thermo-osmotic velocity is much smaller than the particle velocity measured near the upper wall and can be disregarded.

Thermo-osmosis on water-polymer interface has drawn increasing attention lately. Bregulla *et al.* [43] proposed a model to quantify the enthalpy h of the water-polymer interface, and deduced the slip velocity of the thermo-osmosis on such an interface:

$$v_s = -\frac{\Delta H}{\eta}\frac{\lambda}{4\pi r l_p}\frac{\nabla T}{T} \tag{5}$$

where λ is the interaction length, l_p and r are the length and radius of the rod-shaped polymer chains, respectively, and ΔH is the enthalpy of mixing. A negative ΔH leads to a positive χ and the flow moves toward the hot side. In Bregulla's experiment with a relatively hydrophilic polymer (Pluronic F-127) surface, $\chi \sim 10^{-9}$ m^2/s as $\Delta H \sim 10^{-20}$ J. In the case of $\nabla T = 4.05 \times 10^4$ K/m, the thermo-osmotic velocity on their hydrophilic polymer-water interface is 0.2 μm/s based on Eq. (5), which could not be negligible compared to the measured migration speed near the substrate shown in Fig. 3c. Nonetheless, a larger interfacial thermo-osmotic velocity is expected on the hydrophobic polymer surface.

Therefore, in the present rectangular cross-section of the microchannel with a uniform horizontal temperature gradient, only the contribution of the interfacial thermo-osmotic flow on the bottom substrate needs to be considered because the thermo-osmosis on the upper charged metallic surface is much weaker. We use COMSOL (Supplementary material S1) to solve the hydrodynamic creep flow field $v(z)$ in the cross-section of the microchannel (Fig. 3e). As the particle is not involved in the simulation, the simulation velocity field represents the hydrodynamic creep flow caused by the interfacial thermo-osmosis by setting v_s as slip boundary condition. The velocity profile of this creep flow in the central region of the microchannel is determined by a parabolic equation $v(z) = v_s g(z)$, where $g(z) = 0.0012z^2 - 0.08z + 1$ is a geometry parameter determined by the confinement height of the microchannel and obtained by the simulations.

Hence, by substituting $v(z) = v_s g(z)$ into Eq. (1), the equation of the particle migration speed in these experiments becomes:

$$u(z) = \boldsymbol{u}_T + v_s(0.0012z^2 - 0.08z + 1) \tag{6}$$

The two unknown parameters in Eq. (6), *i.e.*, the thermophoretic velocity $\boldsymbol{u}_T$ and the thermo-osmotic velocity v_s were determined by fitting the experimental data. During fitting, the wall effect correctness would be introduced when the particles are close to the wall (Supplementary material S4) [51].

The curves in Fig. 3c are the fits of Eq. (6) for various particles on both hydrophobic and hydrophilic surfaces. The good agreement between the experimental data and the fitting model confirms the reliability of the decoupling method. The hydrodynamic creep flow velocity $v(z)$ caused by thermo-osmosis on two types of substrates and the thermophoretic velocity $\boldsymbol{u}_T$ are plotted separately in Fig. 3f. When the substrate is hydrophobic, the fitted values of $v_s^{hydrophobic}$ for particles with d = 0.2, 0.5, 0.71 and 1.0 μm are 1.45, 1.41, 1.24, and 1.06 μm/s, respectively; the corresponding values for $\boldsymbol{u}_T$ are −0.44, −0.45, −0.42, and −0.39 μm/s, respectively. For a hydrophilic polymer substrate, the fitted values of $v_s^{hydrophilic}$ for particles with d = 0.71 and 1.0 μm are 0.69 and 0.64 μm/s, respectively; and the corresponding values for $\boldsymbol{u}_T$ are −0.39 and −0.37 μm/s, respectively. Although the fitted thermo-osmotic velocity $v_s^{hydrophobic}$ on the hydrophobic surface was approximately-two times larger than that on the hydrophilic surface, the fitted thermophoretic velocities $\boldsymbol{u}_T$ of various particles were very similar.

It is also of interest to estimate how the confinement height of the microchannel influences the flow field $v(z)$ caused by the interfacial thermo-osmosis. The thermo-osmosis generates an interfacial flow from cold to hot on the bottom and a reversed flow far from the wall according to mass conservation. Thus, for a channel with large height, it is easy to know that the reversed flow in the major part of the channel becomes weak. For instance, we estimate that for a microchannel with height about 500 μm the average flow speed in the middle of the channel could reduce to smaller than 0.05 μm/s, which is 1/10 of the particle thermophoretic speed. In this case, the thermo-osmotic flow becomes negligible far from the confinement wall [25,43]. On the contrary, for strong confinement effect with small channel height, the flow speed caused by thermo-osmosis could be much larger than the real particle thermophoretic speed [11]. However, note that the thermal convection effect could become significant when the height of the channel is in the order of a few hundred micrometers [1,24].

3.3. Larger thermo-osmosis enhanced by the intrinsic fluid slip

Fig. 4a shows the thermophoretic velocities $\boldsymbol{u}_T$ (d = 1 μm, red squares) and thermo-osmotic velocity $v_s^{hydrophobic}$ (green circles) under different temperature gradients after decoupling. We can see that both the $\boldsymbol{u}_T$ and $v_s^{hydrophobic}$ vary linearly with the temperature gradient ∇T, which is in agreement with the existing results [22,39,43], as shown in Eq. (2), (3), and (5) as well. As the average temperature in the middle part of the microchannel T = 36.1 °C is constant in all experiments, the thermo-osmotic coefficient χ of the hydrophobic polymer substrate is 8.1 × 10^{-9} m^2/s, which is approximately-three times larger than the thermophoretic effect $TD_T \sim 3 \times 10^{-9}$ m^2/s. As a result, PS particle migration near the hydrophobic substrate was dominated by thermo-osmosis rather than thermophoresis, and exhibited unexpected thermophilic behavior.

It is noteworthy that the thermo-osmotic coefficient χ = 8.1 × 10^{-9} m^2/s of the hydrophobic polymer substrate is 1 – 2 orders of magnitude larger than the reported value of hydrophilic surface (χ = 1.8 × 10^{-10} m^2/s for glass surfaces, and χ = 13 × 10^{-10} m^2/s for Pluronic F-127 covered surfaces) [43]. According to the above decoupled result of $v_s^{hydrophilic}$, the thermo-osmotic coefficient χ of our hydrophilic polymer substrate by the plasma treatment was χ = 4.9 × 10^{-9} m^2/s. The measured thermo-osmotic coefficients χ

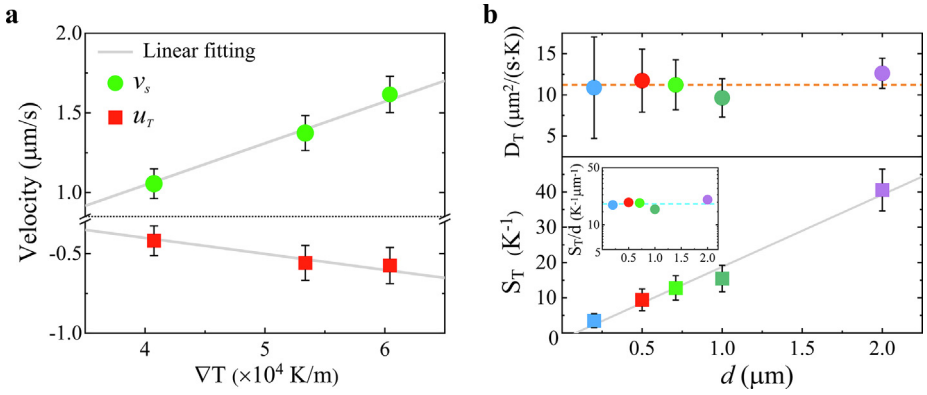

Fig. 4. (a) Thermo-osmotic velocities $v_s^{hydrophobic}$ on the hydrophobic substrate and the thermophoretic velocities $\boldsymbol{u}_T$ of 1 μm particles under various ∇T. Gray lines represent the linear fitting with Eq. (2) and (3), respectively. (b) Size dependence. Top panel: the thermophoretic mobility D_T is approximately constant and independent of particle diameter d. The orange dashed line is the average value of D_T = 11.2 μm²/(s·K). Bottom panel: the Soret coefficient S_T increases linearly with d, where the gray line is the linear fitting of the data. The inset shows S_T/d as a function of d, where the dashed line is the average value of S_T/d = 18 K^{-1} μm^{-1}. (For interpretation of the references to colour in this figure legend, the reader is referred to the web version of this article.)

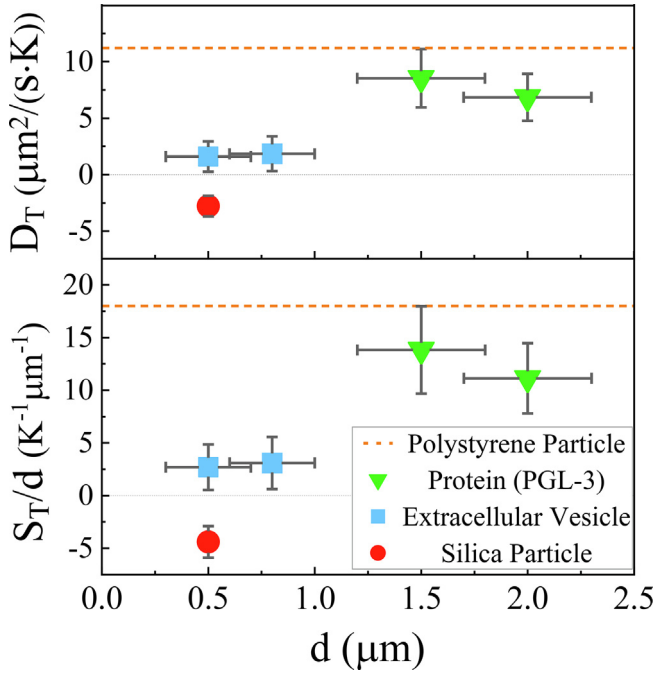

Fig. 5. Top panel: thermophoretic mobility D_T. Bottom panel: normalized Soret coefficient S_T/d of various particles.

on hydrophilic polymer surfaces from this experiment and the experiment of Ref. 41 were one order of magnitude larger than χ on a hydrophilic glass surface. This result indicates the strong contribution of the enthalpy of water-polymer surface on thermo-osmosis based on Eq. (5). The extra enhancement of the thermo-osmosis on the hydrophobic polymer surface in our experiment is 65 % larger than that on the hydrophilic polymer surface, which is also much larger than the thermo-osmosis on the hydrophilic polymer surface (Pluronic F-127) [43]. This extra enhancement suggests an additional effect that has not been reported yet, as these water-polymer surface should have similar enthalpy.

We attribute this extra effect to the intrinsic fluid slip v^*_s on top of the hydrophobic polymer, as shown in the bottom panel of Fig. 3d. Compared to the hydrophilic polymer surface, the apparent thermo-osmotic velocity on a hydrophobic polymer surface, *i.e.*, $v_s^{hydrophobic}$, is enhanced by the intrinsic fluid slip v^*_s in the interfacial layer. Thus, we establish the relation $v_s^{hydrophobic} = v^*_s + v_s^{hydrophilic}$ to describe the contribution of the intrinsic slip. Theoretically, the intrinsic slip v^*_s is related to the slip length b and the shear rate γ, *i.e.*, $v^*_s = b\gamma$ [52]. The slip length on a hydrophobic polymer surface is estimated to be approximately 10 nm, according to the current results [53,54]. Typical shear rate in these experiments is approximately $\gamma \sim v_s/\lambda$ = 10 – 100 s^{-1}, where $v_s \sim 1$ μm based on our measured result and $\lambda \sim$ 10–100 nm based on the typical thickness of the EDL layer. Thus, one finds that the intrinsic fluid slip v^*_s is ~ 0.5 μm/s, which is in excellent agreement with the difference between the measured values of $v_s^{hydrophilic}$ (~0.69 μm/s) and $v_s^{hydrophobic}$ (~1.24 μm/s). Furthermore, as the intrinsic slip is rate dependent, one expects a higher value of v^*_s if a larger temperature gradient is applied. Indeed, as shown in Fig. 4a, the $v_s^{hydrophobic}$ increases from 1.06 to 1.62 μm/s when the temperature gradient is enlarged 50 %, which supports the argument of the intrinsic slip on the hydrophobic polymer surface.

Such a large range of thermo-osmotic coefficient adjusting by surface hydrophilicity might provide a thermo-osmosis-mediated method for enhancing interfacial flow used in opto-thermophoretic manipulation [9–11]. Recently, Fu *et al.* unveiled that the thermo-osmosis of a hydrophobic surface is greatly amplified by the intrinsic slip. They proposed that the thermo-osmotic coefficient χ of the hydrophobic surface could reach 10^{-8} to 10^{-6} m^2/s [55]. Although the hydrophobic substrate in our experiment has a relatively small contact angle (θ = 110°), the measured thermo-osmotic coefficient χ = 8.1 × 10^{-9} m^2/s has reached the lower value (10^{-8} m^2/s) of the theoretical prediction. It is hypothesized that even larger χ could be obtained using superhydrophobic surface [56], through which the interfacial thermo-osmosis could be significantly promoted. We notice recent progress of low-cost methods to fabricate superhydrophobic surfaces [57–59], which could help achieve high thermo-osmosis in future applications. Considering that the molecular mechanism of the thermo-osmosis on various interfaces is remarkably attractive lately [55,60–62], our results could help better understand of the mechanism by providing the first experimental evidence for such a large thermo-osmotic coefficient χ of the hydrophobic surface.

3.4. Size dependence of the Soret Coefficient

The dependence of thermophoresis on the particle size has been a controversial issue. Duhr and Braun [29] reported that the thermophoretic mobility D_T increased linearly with the particle size d (20 nm ≤ d ≤ 2000 nm), and the Soret coefficient S_T (defined as $S_T = -D_T/D$, where D is the diffusion coefficient) changed linearly with d^2

for PS particles. While Braibanti [41] found that particles with a diameter 20 nm $\leq d \leq$ 500 nm show a constant D_T and a linear relationship with $S_T \sim d$. Based on the decoupled results, the thermophoretic mobility D_T of different particles under ∇T = 4.05 $\times$ 10^4 K/m are plotted in Fig. 4b, showing an average value of D_T = 11.2 $\mu m^2/(s{\cdot}K)$. We find that the measured data of D_T appear to be constant and independent on d, suggesting that the Soret coefficient S_T increases linearly with d. Our result of the linear relation $S_T \sim d$ supports the recent experimental results reported in [35–37,39,41], thus might help resolve the controversy of the size dependence of the thermophoresis and the Soret coefficient. Furthermore, our finding differs from the result of Zhou *et al*., who used a similar experimental system and reported a linear dependence and a sign change of D_T [38]. We stress that the existence of the hydrodynamic creep flow caused by interfacial thermo-osmosis could introduce dramatic error to the measured thermophoretic velocity of particles, as space confinement is prevalent in these experiments. For instance, our results show that the thermo-osmotic effect of the wall could exceed the thermophoresis of the particle. Moreover, this study reveals the circulation flow that might be relevant to the thermophoretic direction controversy. Without decoupling, it is impossible to quantify the motions of thermophoresis and thermo-osmosis and to clarify their mechanisms.

To compare the measured S_T with other results, we plot the values of S_T/d and confirm that S_T/d = 18.0 K^{-1} μm^{-1} is approximately constant. This result is two to four times larger than many reported valuites (approximately $S_T/d \sim$ 4.2 – 7.8 $K^{-1}\mu m^{-1}$) [36,41] at a similar average temperature (Supplementary material S5). We suspect that the reported results underestimated S_T if the background flow due to thermo-osmotic flow was not entirely removed. Besides, in Ref. [39], a nonionic surfactant Triton X100 was used to stabilize the particles, forming a monolayer on the particle surface. Tsuji *et al*. reported that the added surfactant would reduce the thermophoresis of the PS particles [63]. It is remarkable that our results are in agreement with the data of Helden *et al*. [37], who obtained S_T/d = 22.2 $K^{-1}\mu m^{-1}$ (Supplementary material S5).

3.5. Large difference of thermophoretic mobilities among various particles

The distinct thermophoretic responses of different particles could be used to selectively separate the particles of interest from other samples, which has been shown as a promising technique lately [15,17,18]. The technique relies on a large difference in the thermophoretic mobilities among the particles that need to be separated. This method can be used to separate bio-particles, such as proteins and EVs, because the microfluidic chip works at T = 36.1 °C, which is very close to the human body temperature. By decoupling the effects of particle thermophoresis and interfacial thermo-osmosis, our method can accurately determine the pure thermophoretic mobility of the bio-particles and the Soret coefficient. Thus, the thermophoretic motion of PGL-3 protein granules and EVs were measured. Fig. 5 and Table 1 show the measured results, where protein PGL-3 granules and EV have a positive Soret coefficient, the same as PS particles. The P granules of Caenorhabditis elegans are a genetic model for studying RNA/protein condensates. The PGL-3 is a core defining component of P granules, which plays a vital role in cell biology and RNA metabolism [64,65]. The thermophoretic mobility D_T and the normalized Soret coefficient S_T/d of PGL-3 were measured to be 7.8 $\mu m^2/(s{\cdot}K)$ and 12.5 K^{-1} μm^{-1}, respectively. Iacopini *et al.* [26] reported that a protein called lysozyme has $S_T/d \sim$ 10 K^{-1} μm^{-1} at T = 36 ℃, close to our result. Braun *et al.* [5,6] obtained the binding constants of proteins based on their relatively large thermophoresis. The EVs have a much smaller thermophoretic mobility D_T = 1.8 $\mu m/(s{\cdot}K)$, corresponding to S_T/d = 2.9 K^{-1} μm^{-1}. Thus, the normalized Soret coefficient of the hydrophobic PGL-3 particles is approximately-four times larger than that of hydrophilic EVs. Talbot *et al.* [66] examined the thermophoretic behavior of vesicles and attributed the small mobility to the surface chemistry of lipid head groups. However, in contrast to the unilamellar lipid vesicles they used, the EVs used in this experiment were extracted from the mesenchymal stem cells (MSC) and had more complex surface properties [67]. Silica particles manifest an opposite thermophoretic motion compared to other particles, and the S_T is negative. Ning *et al.* [31,34] and Weinert *et al.* [25] also found a negative thermophoresis for silica particles. The absolute values of the D_T and S_T/d are also much smaller than those of PS particles or protein granules.

Interestingly, the large difference between the EV and protein might also be due to the larger slip caused by the hydrophobic surface of the protein. Similar to the hydrophobic substrate, where the interfacial flow is enhanced by the intrinsic slip [55], the solvent molecules in the interfacial layer of the hydrophobic protein surface move rapidly to the hot side under the temperature gradient, resulting in a large positive thermophoretic mobility compared to the hydrophilic EV. This implies that bio-particles with different hydrophilicity might manifest large differences in thermophoretic mobilities. Such a large difference in thermophoretic mobilities highlights the possibility of using thermophoresis to separate bio-particles based on the microfluidic method. There are still many issues needed to be understood on how the surface properties and molecular compositions influence the thermophoretic motion of particles, though some recent studies have shown attractive mechanism and phenomena [66]. It is also interesting to paid attention to the effect of surface heterogeneity on the thermophoresis of bio-particles. Such effect is related to complicated interfacial mechanisms, yet has not been well understood. Future study on particle thermophoresis could focus on the impact of particle surface heterogeneity. To obtain heterogeneous particles, possible strategies include modifying functional groups on particle surface [68] and synthesize anisotropic particles directly [69].

Table 1
Thermophoresis of different particles.

$\nabla T = 4.05 \times 10^4$ $K/m$and T = 36.1 °C	d (μm)	u_T(μm/s)	$D_T(\mu m^2/s{\cdot}K)$	$S_T(K^{-1})$	$S_T/d(K^{-1}\mu m^{-1})$
Polystyrene	0.2 ~ 2	−0.45	11.2	3.5 – 40.6	18.0
Silica	0.5	0.11	−2.7	−2.2	−4.4
Protein [a]	1.5	−0.34	8.6	20.7	13.8
	2	−0.28	6.9	22.2	11.1
Extracellular vesicle [b]	0.5	−0.07	1.7	1.3	2.7
	0.8	−0.08	1.9	2.5	3.1

[a] PGL-3 granules, the RGG-domain proteins, a kind of germ granules in Caenorhabditis elegans.
[b] Mesenchymal stem cell (MSC) extracellular vesicles. The size of prepared EVs is non-uniform, and the size distribution varies from 0.1 to 0.8 μm. Only the thermophoresis of particles $d \geq$ 0.5 μm was measured owing to the optical limitations.

4. Conclusions

This study established a uniform and stable temperature gradient in a microfluidic channel to study the migration of various nano/microparticles under this temperature gradient. By decoupling the contributions of the particle thermophoresis and the interfacial thermo-osmosis of the substrate, we explained the coexistence of thermophilic and thermophobic migrations of particles and quantify the size dependence of the Soret coefficient *ST*. Existing results of the normalized Soret coefficient manifested controversial size dependence [28,41] and scattered data ($ST/d \sim 4$ – 22 $K^{-1}\mu m^{-1}$, Supplementary material S5) [35–37,41]. This paper reported a constant $ST/d = 18.0\ K^{-1}\ \mu m^{-1}$ for PS particles with sizes ranging from 200 nm to 2 μm. This Soret coefficient is larger than many previous data [35,36,41,63]. Therefore, it is speculated that some previous studies might underestimate the values as the influence of thermo-osmotic flow was neglected. Indeed, our experiment provided the first experimental evidence of the large thermo-osmosis on a hydrophobic polymer substrate. The thermo-osmotic coefficient on the hydrophobic polymer surface, which is $\chi = 8.1 \times 10^{-9}\ m^2/s$, is 1 – 2 orders of magnitude larger than previously reported values on a hydrophilic glass surface ($\chi = 1.8 \times 10^{-10}\ m^2/s$) [22,43], and much larger than that on a hydrophilic polymer surface ($\chi = 1.3 \times 10^{-9}\ m^2/s$ from Ref. 41, $\chi = 4.9 \times 10^{-9}\ m^2/s$ from our data). Recent result from Bregulla *et al.* [43] has indicated the vital contribution of the enthalpy of hydrophilic water-polymer surface on thermo-osmosis. On the basis of their work, this result suggests the effect of the intrinsic slip on the hydrophobic polymer surface, which could further enlarge the interfacial thermo-osmosis by 65 %. Such hydrophilicity mediated mechanism can help understand the different thermophoretic mobilities among various bio-particles because the particle thermophoresis originates from the interfacial hydrodynamics as well. We found that the normalized Soret coefficient of the hydrophobic PGL-3 particles is approximately-four times larger than that of hydrophilic EVs. These results shed light on using the synergistic effects of thermophoresis and thermo-osmosis to detect and separate bio-particles and enhancing thermal migration by the slip on the hydrophobic surface. Our work thus provides new strategies for opto-thermophoretic manipulation [9–13] and photothermal nanorobots [18–20].

CRediT authorship contribution statement

Haolan Xu: Conceptualization, Methodology, Investigation, Formal analysis, Writing – original draft. **Xu Zheng:** Conceptualization, Methodology, Resources, Writing – review & editing, Funding acquisition, Project administration. **Xinghua Shi:** Conceptualization, Methodology, Resources, Writing – review & editing, Funding acquisition, Supervision.

Data availability

Data will be made available on request.

Declaration of Competing Interest

The authors declare that they have no known competing financial interests or personal relationships that could have appeared to influence the work reported in this paper.

Acknowledgments

We are grateful for the financial support from the Strategic Priority Research Program of the Chinese Academy of Sciences (XDB36000000 and XDB22040403), the CAS Key Research Program of Frontier Sciences (QYZDB-SSW-JSC036), the Natural Science Foundation of Beijing (2184130 and 1202023), and the National Natural Science Foundation of China (11672079, 12072082, 12072350, 11832017, and 12125202).

Appendix A. Supplementary data

Supplemental movies of particles' migration, and the details of Supplementary material (PDF): S1 Working Mechanism of Microfluidic Chip and Numerical Simulation, S2 Contact Angle Measurements, S3 Temperature-dependent Variation of the Fluorescence Intensity, S4 Hydrodynamic Wall Effect, S5 Size Dependence of Soret Coefficient. Supplementary data to this article can be found online at https://doi.org/10.1016/j.jcis.2023.01.112.

References

[1] D. Braun, A. Libchaber, Trapping of DNA by thermophoretic depletion and convection, Phys. Rev. Lett. 89 (18) (2002) 188103.
[2] C.B. Mast, D. Braun, Thermal trap for DNA replication, Phys. Rev. Lett. 104 (18) (2010) 188102.
[3] H.R. Jiang, N. Yoshinaga, M. Sano, Active motion of a Janus particle by self-thermophoresis in a defocused laser beam, Phys. Rev. Lett. 105 (26) (2010) 268302.
[4] C. Bechinger, R. Di Leonardo, H. Löwen, C. Reichhardt, G. Volpe, G. Volpe, Active Particles in Complex and Crowded Environments, Rev. Mod. Phys. 88 (4) (2016).
[5] C.J. Wienken, P. Baaske, U. Rothbauer, D. Braun, S. Duhr, Protein-binding assays in biological liquids using microscale thermophoresis, Nat. Commun. 1 (2010) 100.
[6] J.A.C. Stein, A. Ianeselli, D. Braun, Kinetic Microscale Thermophoresis for Simultaneous Measurement of Binding Affinity and Kinetics, Angew. Chem. Int. Ed. Engl. 60 (25) (2021) 13988–13995.
[7] T. Cui, S. Wu, Y. Sun, J. Ren, X. Qu, Self-Propelled Active Photothermal Nanoswimmer for Deep-Layered Elimination of Biofilm In Vivo, Nano Lett. 20 (10) (2020) 7350–7358.
[8] C.M. Maier, M.A. Huergo, S. Milosevic, C. Pernpeintner, M. Li, D.P. Singh, D. Walker, P. Fischer, J. Feldmann, T. Lohmuller, Optical and Thermophoretic Control of Janus Nanopen Injection into Living Cells, Nano Lett. 18 (12) (2018) 7935–7941.
[9] L. Lin, M. Wang, X. Peng, E.N. Lissek, Z. Mao, L. Scarabelli, E. Adkins, S. Coskun, H.E. Unalan, B.A. Korgel, L.M. Liz-Marzan, E.L. Florin, Y. Zheng, Opto-thermoelectric nanotweezers, Nat. Photonics 12 (4) (2018) 195–201.
[10] S. Liu, L. Lin, H.B. Sun, Opto-Thermophoretic Manipulation, ACS Nano 15 (4) (2021) 5925–5943.
[11] M. Franzl, F. Cichos, Hydrodynamic manipulation of nano-objects by optically induced thermo-osmotic flows, Nat. Commun. 13 (1) (2022) 656.
[12] M. Trivedi, D. Saxena, W.K. Ng, R. Sapienza, G. Volpe, Self-organized lasers from reconfigurable colloidal assemblies, Nat. Phys. 18 (8) (2022) 939–944.
[13] H. Ding, Z. Chen, P.S. Kollipara, Y. Liu, Y. Kim, S. Huang, Y. Zheng, Programmable Multimodal Optothermal Manipulation of Synthetic Particles and Biological Cells, ACS Nano (2022).
[14] Q. Dai, J. Yan, A. Sadeghi, W. Huang, X. Wang, M.M. Khonsari, Creating lifting force in liquids via thermal gradients, J. Colloid Interface Sci. 629 (Pt B) (2022) 245–253.
[15] J. Deng, F. Tian, C. Liu, Y. Liu, S. Zhao, T. Fu, J. Sun, W. Tan, Rapid One-Step Detection of Viral Particles Using an Aptamer-Based Thermophoretic Assay, J. Am. Chem. Soc. 143 (19) (2021) 7261–7266.
[16] C. Liu, J. Zhao, F. Tian, L. Cai, W. Zhang, Q. Feng, J. Chang, F. Wan, Y. Yang, B. Dai, Y. Cong, B. Ding, J. Sun, W. Tan, Low-cost thermophoretic profiling of extracellular-vesicle surface proteins for the early detection and classification of cancers, Nat. Biomed. Eng. 3 (3) (2019) 183–193.
[17] J. Deng, S. Zhao, J. Li, Y. Cheng, C. Liu, Z. Liu, L. Li, F. Tian, B. Dai, J. Sun, One-Step Thermophoretic AND Gate Operation on Extracellular Vesicles Improves Diagnosis of Prostate Cancer, Angew. Chem. Int. Ed. Engl. 61 (33) (2022) e202207037.
[18] X. Liu, W. Chen, D. Zhao, X. Liu, Y. Wang, Y. Chen, X. Ma, Enzyme-Powered Hollow Nanorobots for Active Microsampling Enabled by Thermoresponsive Polymer Gating, ACS Nano (2022).
[19] P.L. Venugopalan, B. Esteban-Fernandez de Avila, M. Pal, A. Ghosh, J. Wang, Fantastic Voyage of Nanomotors into the Cell, ACS Nano 14 (8) (2020) 9423–9439.
[20] S. Cao, J. Shao, H. Wu, S. Song, M.T. De Martino, I.A.B. Pijpers, H. Friedrich, L. Abdelmohsen, D.S. Williams, J.C.M. van Hest, Photoactivated nanomotors via aggregation induced emission for enhanced phototherapy, Nat. Commun. 12 (1) (2021) 2077.
[21] E. Ruckenstein, Can phoretic motions be treated as interfacial tension grandient driven phenomena?, J Colloid Interface Sci. 83 (1) (1981) 77–81.

[22] B.V. Derjaguin, N.V. Churaev, V.M. Muller, Surface Forces, Springer New York, NY (1987), https://doi.org/10.1007/978-1-4757-6639-4.
[23] J.L. Anderson, Colloid Transport by Interfacial Forces, Ann. Rev. Fluid Mech. 21 (1989) 61–99.
[24] A. Würger, Thermophoresis in colloidal suspensions driven by Marangoni forces, Phys. Rev. Lett. 98 (13) (2007) 138301.
[25] F.M. Weinert, D. Braun, Observation of slip flow in thermophoresis, Phys. Rev. Lett. 101 (16) (2008) 168301.
[26] S. Iacopini, R. Piazza, Thermophoresis in protein solutions, Europhysics Letters (EPL) 63 (2) (2003) 247–253.
[27] S.A. Putnam, D.G. Cahill, Transport of nanoscale latex spheres in a temperature gradient, Langmuir 21 (12) (2005) 5317–5323.
[28] S. Duhr, D. Braun, Thermophoretic Depletion Follows Boltzmann Distribution, Phys. Rev. Lett. 96 (16) (2006).
[29] S. Duhr, D. Braun, Why molecules move along a temperature gradient, PNAS 103 (52) (2006) 19678–19682.
[30] S. Iacopini, R. Rusconi, R. Piazza, The "macromolecular tourist": universal temperature dependence of thermal diffusion in aqueous colloidal suspensions, Eur. Phys. J. E Soft Matter 19 (1) (2006) 59–67.
[31] H. Ning, J. Buitenhuis, J.K. Dhont, S. Wiegand, Thermal diffusion behavior of hard-sphere suspensions, J. Chem. Phys. 125 (20) (2006) 204911.
[32] J.K.G. Dhont, S. Wiegand, S. Duhr, D. Braun, Thermodiffusion of Charged Colloids Single-Particle Diffusion, Langmuir 23 (2007).
[33] D.G.C. Shawn, A. Putnam, G.C.L. Wong, Temperature Dependence of Thermodiffusion in Aqueous Suspensions of Charged Nanoparticles, Langmuir (2007).
[34] H. Ning, J.K.G. Dhont, S. Wiegand, Thermal-Diffusive Behavior of a Dilute Solution of Charged Colloids, Langmuir 24 (6) (2008).
[35] H.R. Jiang, H. Wada, N. Yoshinaga, M. Sano, Manipulation of colloids by a nonequilibrium depletion force in a temperature gradient, Phys. Rev. Lett. 102 (20) (2009) 208301.
[36] K.A. Eslahian, A. Majee, M. Maskos, A. Wurger, Specific salt effects on thermophoresis of charged colloids, Soft Matter 10 (12) (2014) 1931–1936.
[37] L. Helden, R. Eichhorn, C. Bechinger, Direct measurement of thermophoretic forces, Soft Matter 11 (12) (2015) 2379–2386.
[38] Y. Zhou, C. Yang, Y.C. Lam, X. Huang, Thermophoresis of charged colloidal particles in aqueous media – Effect of particle size, Int. J. Heat Mass Transf. 101 (2016) 1283–1291.
[39] A. Würger, Thermal non-equilibrium transport in colloids, Rep. Prog. Phys. 73 (12) (2010).
[40] Y. Yang, X. Zhang, Z. Tian, G. Deissmann, D. Bosbach, P. Liang, M. Wang, Thermodiffusion of ions in nanoconfined aqueous electrolytes, J. Colloid Interface Sci. 619 (2022) 331–338.
[41] M. Braibanti, D. Vigolo, R. Piazza, Does thermophoretic mobility depend on particle size?, Phys Rev. Lett. 100 (10) (2008) 108303.
[42] M. Holub, M. Adobes-Vidal, A. Frutiger, P.M. Gschwend, S.E. Pratsinis, D. Momotenko, Single-Nanoparticle Thermometry with a Nanopipette, ACS Nano 14 (6) (2020) 7358–7369.
[43] A.P. Bregulla, A. Wurger, K. Gunther, M. Mertig, F. Cichos, Thermo-Osmotic Flow in Thin Films, Phys. Rev. Lett. 116 (18) (2016) 188303.
[44] S. Ketzetzi, J. de Graaf, R.P. Doherty, D.J. Kraft, Slip Length Dependent Propulsion Speed of Catalytic Colloidal Swimmers near Walls, Phys. Rev. Lett. 124 (4) (2020) 048002.
[45] D. Vigolo, R. Rusconi, R. Piazza, H.A. Stone, A portable device for temperature control along microchannels, Lab Chip 10 (6) (2010) 795–798.
[46] D. Vigolo, R. Rusconi, H.A. Stone, R. Piazza, Thermophoresis: microfluidics characterization and separation, Soft Matter 6 (15) (2010).
[47] Y. Zhao, C. Zhao, J. He, Y. Zhou, C. Yang, Collective effects on thermophoresis of colloids: a microfluidic study within the framework of DLVO theory, Soft Matter 9 (32) (2013).
[48] X. Zheng, Z.-H. Silber-Li, Measurement of velocity profiles in a rectangular microchannel with aspect ratio α = 0.35, Exp. Fluids 44 (6) (2008) 951–959.
[49] X. Zheng, G.-P. Kong, Z.-H. Silber-Li, The influence of nano-particle tracers on the slip length measurements by microPTV, Acta Mechanica Sinica 29 (3) (2013) 411–419.
[50] D. Ross, M. Gaitan, L.E. Locascio, Temperature Measurement in Microfluidic Systems Using a Temperature-Dependent Fluorescent Dye, Anal. Chem. 73 (17) (2001) 4117–4123.
[51] A. Wurger, Hydrodynamic Boundary Effects on Thermophoresis of Confined Colloids, Phys. Rev. Lett. 116 (13) (2016) 138302.
[52] C. Neto, D.R. Evans, E. Bonaccurso, H.-J. Butt, V.S.J. Craig, Boundary slip in Newtonian liquids: a review of experimental studies, Rep. Prog. Phys. 68 (12) (2005) 2859–2897.
[53] L. Joly, C. Ybert, L. Bocquet, Probing the nanohydrodynamics at liquid-solid interfaces using thermal motion, Phys. Rev. Lett. 96 (4) (2006) 046101.
[54] C. Cottin-Bizonne, B. Cross, A. Steinberger, E. Charlaix, Boundary Slip on Smooth Hydrophobic Surfaces: Intrinsic Effects and Possible Artifacts, Phys. Rev. Lett. 94 (5) (2005).
[55] L. Fu, S. Merabia, L. Joly, What Controls Thermo-osmosis? Molecular Simulations Show the Critical Role of Interfacial Hydrodynamics, Phys. Rev. Lett. 119 (21) (2017) 214501.
[56] D.M. Huang, C. Sendner, D. Horinek, R.R. Netz, L. Bocquet, Water slippage versus contact angle: a quasiuniversal relationship, Phys. Rev. Lett. 101 (22) (2008) 226101.
[57] F. Beshkar, H. Khojasteh, M. Salavati-Niasari, Recyclable magnetic superhydrophobic straw soot sponge for highly efficient oil/water separation, J. Colloid Interface Sci. 497 (2017) 57–65.
[58] F. Beshkar, M. Salavati-Niasari, O. Amiri, Superhydrophobic–superoleophilic copper–graphite/styrene–butadiene–styrene based cotton filter for efficient separation of oil derivatives from aqueous mixtures, Cellul. 27 (8) (2020) 4691–4705.
[59] F. Beshkar, M. Salavati-Niasari, O. Amiri, A reliable hydrophobic/superoleophilic fabric filter for oil–water separation: hierarchical bismuth/purified terephthalic acid nanocomposite, Cellul. 27 (16) (2020) 9559–9575.
[60] R. Ganti, Y. Liu, D. Frenkel, Molecular Simulation of Thermo-osmotic Slip, Phys. Rev. Lett. 119 (3) (2017) 038002.
[61] R. Ganti, Y. Liu, D. Frenkel, Hamiltonian Transformation to Compute Thermo-osmotic Forces, Phys. Rev. Lett. 121 (6) (2018) 068002.
[62] P. Anzini, G.M. Colombo, Z. Filiberti, A. Parola, Thermal Forces from a Microscopic Perspective, Phys. Rev. Lett. 123 (2) (2019) 028002.
[63] T. Tsuji, S. Saita, S. Kawano, Dynamic Pattern Formation of Microparticles in a Uniform Flow by an On-Chip Thermophoretic Separation Device, Phys. Rev. Appl 9 (2) (2018) 024035.
[64] S.T. Aoki, A.M. Kershner, C.A. Bingman, M. Wickens, J. Kimble, PGL germ granule assembly protein is a base-specific, single-stranded RNase, PNAS 113 (5) (2016) 1279–1284.
[65] G. Zhang, Z. Wang, Z. Du, H. Zhang, mTOR Regulates Phase Separation of PGL Granules to Modulate Their Autophagic Degradation, Cell 174 (6) (2018) 1492–1506.
[66] E.L. Talbot, J. Kotar, L. Parolini, L. Di Michele, P. Cicuta, Thermophoretic migration of vesicles depends on mean temperature and head group chemistry, Nat. Commun. 8 (2017) 15351.
[67] R. Kalluri, V.S. LeBleu, The biology, function, and biomedical applications of exosomes, Science 367 (6478) (2020).
[68] S.S. Pradhan, S. Saha, Advances in design and applications of polymer brush modified anisotropic particles, Adv. Colloid Interface Sci. 300 (2022) 102580.
[69] M. Panahi-Kalamuei, S. Alizadeh, M. Mousavi-Kamazani, M. Salavati-Niasari, Synthesis and characterization of CeO 2 nanoparticles via hydrothermal route, J. Ind. Eng. Chem. 21 (2015) 1301–1305.